Proceedings of IMECE2009
2009 ASME International Mechanical Engineering Congress and Exposition
November 13-19, Lake Buena Vista, Florida, USA

IMECE2009-10134

INVERSE HEAT CONDUCTION IN A COMPOSITE SLAB WITH PYROLYSIS EFFECT AND TEMPERATURE-DEPENDENT THERMOPHYSICAL PROPERTIES

Jianhua Zhou, Yuwen Zhang, J. K. Chen and Z. C. Feng
Department of Mechanical and Aerospace Engineering
University of Missouri
Columbia, MO 65211, USA
Email: zhangyu@missouri.edu

ABSTRACT

The inverse heat conduction problem (IHCP) in a one-dimensional composite slab with rate-dependent pyrolysis chemical reaction and outgassing flow effects is investigated using the conjugate gradient method (CGM). The thermal properties of the composites are considered to be temperature-dependent, which makes the IHCP a nonlinear problem. The inverse problem is formulated in such a way that the front-surface heat flux is chosen as the unknown function to be recovered, and the front-surface temperature is computed as a by-product of the IHCP algorithm, which uses back-surface temperature and heat flux measurements. The proposed IHCP formulation is then applied to solve the IHCP in an organic composite slab whose front surface is subjected to high intensity periodic laser heating. It is shown that an extra temperature sensor located at an interior position is necessary since the organic composites usually possess a very low thermal conductivity. It is also found that the frequency of the periodic laser heating flux plays a dominant role in the inverse solution accuracy. In addition, the robustness of the proposed algorithm is demonstrated by its capability in handling the case of thermophysical properties with random errors.

1. INTRODUCTION

Advanced composites are materials in which two (or more) constituents are engineered to produce properties that would not be attained by conventional means [1]. Composite materials are widely used for aircraft and missile cases due to their lightweight and durability. To defeat the invasion of the enemy military object, High Energy Laser (HEL) weapons can be employed because they offer the advantages of remote delivery of energy at the speed of light onto a small spot on military target. During laser irradiation, it is critical to know the temperature at the heated front target surface in order to accurately understand damage mechanism. However, the heated front-surface is either inaccessible or too hot so that it is unsuitable for attaching a sensor. Similar problems are found in some laser manufacturing processes [2]. Under these circumstances, the heated (front) surface temperature can be determined indirectly by solving an inverse heat conduction problem (IHCP) [3-5] based on the transient temperature and/or heat flux measured at the back surface.

In the mathematical formulation of the inverse problem, either temperature or heat flux can be measured at the back surface. Most researchers prefer temperature measurements because temperature can be measured with fewer uncertainties compared to the heat flux measurements [6-9]. However, recent studies have showed that using measured heat flux as additional information in the formulation of an IHCP can make the solution less prone to the inherent instability of the ill-posed problem of inverse heat conduction [10, 11].

Although IHTPs have been extensively studied for different applications in the past (e.g., [12-20]), little work has been done for periodic laser irradiation to a remote surface. The laser energy is delivered to the surface in a periodic way due to target-spinning or atmosphere variation. Since the formulation of the IHCP is quite subjective, it is necessary to determine which formulation is more appropriate for applications with a periodic heat flux, which may pose extra difficulties in the solution of the inverse problems.

Recently, the authors proposed a robust and error-insensitive IHCP algorithm to reconstruct the front-surface heating condition with back-surface measurement data [21, 22]. It was demonstrated that the best solution can be obtained by choosing the front-surface heat flux as the unknown function

and using the temperature measurement data as the boundary condition at back surface while the heat flux measurement data is employed in the objective function. However, the applicability of the authors' work is limited to pure conduction cases. To the best of the authors' knowledge, little is done for the inverse problem in composite materials subjected to laser heating. For composites, when the temperature is elevated to the pyrolysis point, the composite material undergoes chemical decomposition. Meanwhile, the decomposing process gives off gaseous byproducts that flow from the pyrolysis zone toward the composite front surface [23, 24]. Furthermore, the thermal conductivities of composite materials are usually very low. It will be very difficult, if not impossible, to recover the heating condition at remote surface based on the information measured at accessible surface.

In this study, the IHCP in composite materials with pyrolysis effect and temperature-dependent thermophysical properties is investigated using the conjugate gradient method (CGM). The proposed inverse model incorporates many important mechanisms, including temperature-dependent thermal properties, rate-dependent chemical reaction, pyrolysis byproduct outgassing, etc. Parametric studies are performed to determine the optimum locations of the measurement points for periodic laser heating with different frequencies. The robustness of the proposed algorithm is also demonstrated by its strong ability in handling the case of thermophysical properties with random errors.

NOMENCLATURE

A	frequency factor
B	a parameter related to activation energy, K
c	mass specific heat, J/(kg·K)
c_{pg}	mass specific heat of gas at constant pressure, J/(kg·K)
C	volume specific heat, J/(m^3·K)
D	diameter of the gas flow channel, D=2 R_c , m
f	frequency of periodic laser heating, Hz
f_r	friction factor
$G(x, t)$	heat source due to the convective heat exchange between the pyrolysis gas and the solid part, W/m^3
h_{gas}	convection heat transfer coefficient between the gaseous byproducts and the solid part of the composite, W/(m^2·K)
ΔH	chemical reaction heat, J/kg
k	thermal conductivity, W/(m·K)
L	thickness of 1-D composite material, m
M	order of decomposition chemical reaction
Ma	Mach number
Nu_D	Nusselt number
q	heat flux, W/m^2
$q_1(t)$	heat flux at front surface, W/m^2
$\Delta q[L,t;d^k(t)]$	heat flux variation, which is sometimes simplified as $\Delta q(d^k)$
$Q(x, t)$	heat source arising from the pyrolysis decomposition, W/m^3
S	objective functions
$\nabla S[q_1^k(t)]$	gradient direction of objective functional at iteration k
$\Delta S[q_1(t)]$	objective function variation
R_c	radius of the gas flow channel, m
R_f	outer radius of the fiber, m
R_g	gas constant, J/(kg·K)
t	time, s
t_f	final time, s
t_{pyro}	pyrolysis onset time, s
T	temperature, K
T_0	initial temperature, K
$T_1(t)$	front surface temperature, K
T_∞	ambient temperature, K
T_g	temperature of the pyrolysis gas, K
T_{g0}	gas stagnation temperature, K
$\Delta T[x,t;q_1(t)]$	temperature variation, which is sometimes simplified as ΔT
υ_g	gas flow velocity, m/s
x	spatial coordinate variable, m
$Y_{qL}(t)$	measurement heat flux at the back surface, W/m^2
$Y_{T1}(t)$	temperature reading at interior location, K
$Y_{TL}(t)$	measurement temperature at the back surface, K

Greek symbols

α	fraction of the decomposed material
β^k	search step size at iteration level k
χ	tolerance used to stop the CGM iteration procedure
δ_q	standard deviations of the heat flux measurement
δ_T	standard deviations of the temperature measurement
ε	surface emissivity
κ	specific heat ratio of the pyrolysis gas
γ^k	conjugate coefficient at iteration level k
$\lambda(x,t)$	Lagrange multiplier
ρ	density, kg/m^3
σ	Stefan-Boltzmann constant, σ = 5.67×10^{-8} W/(m^2·K^4)

ω	random variable between -1 and 1
ξ	perturbed variable
Superscripts	
k	iteration level
Subscripts	
0	initial
f	fiber
g	gas
m	matrix
max	maximum
q	heat flux
T	temperature

2. MODEL DESCRIPTION

For a laser beam with flat-top profile, if the beam size is much larger than the thickness of a heated target, the IHCP can be treated as a one-dimensional problem. To illustrate the methodology of the inverse heat transfer algorithms employed in this study, a finite composite slab with a thickness of L, as shown in Fig. 1, is considered. The black regions represent fibers; the gray regions denote the matrix. Initially, the slab is uniformly at temperature T_0 and is subjected to a high intensity laser heating from $t = 0^+$ at its front surface ($x = 0$). Before the pyrolysis occurs, only pure conduction takes place in the composite. When the temperature of the composite is elevated to the pyrolysis temperature, the composite material undergoes chemical decomposition. Meanwhile, the decomposing process gives off gaseous byproducts that flow outward from the pyrolysis zone to the composite surface [the white regions in Fig. 1 represent the gas flow channels]. Thus, there is convection heat exchange between the solid part of the composite and the pyrolysis gas. Each gas flow channel, together with its surrounding material, constitutes an element (shown by the dash-line rectangular box in Fig. 1).

The purpose of the IHCP is to reconstruct the heat flux $q_1(t)$ and temperature $T_1(t)$ at the front surface of the composite material based on the measured temperature and heat flux at the back surface, or/and the temperature readings at some interior locations if necessary. Due to the fact that temperature measurement contains much less errors compared to the heat flux measurement [6-9], the back surface temperature $Y_{TL}(t)$ is used as the boundary condition, and the back surface heat flux $Y_{qL}(t)$ and the temperature reading at interior location $Y_{T1}(t)$ are adopted in the objective function.

In the reminder of this section, the mathematical formulations for the direct, inverse, sensitivity and adjoint problems required for the CGM solution of the inverse problem in composites will be derived.

2.1 The direct problem

The direct problem can be expressed as follows:

$$C(T)\frac{\partial T}{\partial t} = \frac{\partial}{\partial x}\left[k(T)\frac{\partial T}{\partial x}\right] + Q(x,t) + G(x,t) \qquad (1)$$

$$T = T_0 \quad \text{for} \quad 0 \le x \le L, \quad t = 0 \qquad (2)$$

$$-k(T)\frac{\partial T}{\partial x} = q_1(t) \quad \text{for} \quad x = 0,\ t > 0 \qquad (3)$$

$$T(L,t) = Y_{TL}(t) \quad \text{for} \quad x = L,\ t > 0 \qquad (4)$$

where t is time; T is temperature; x is coordinate variable; C and k are the volume specific heat and thermal conductivity of the material (fiber), respectively; $Q(x,t)$ is the heat generation arising from the pyrolysis decomposition; $G(x,t)$ is the heat source due to the convective heat exchange between the pyrolysis gas and the solid part; T_0 is initial temperature; L is thickness of the composites; $q_1(t)$ is the observed heat flux at front surface (x=0); $Y_{TL}(t)$ is the temperature at back-surface which is a measurement quantity.

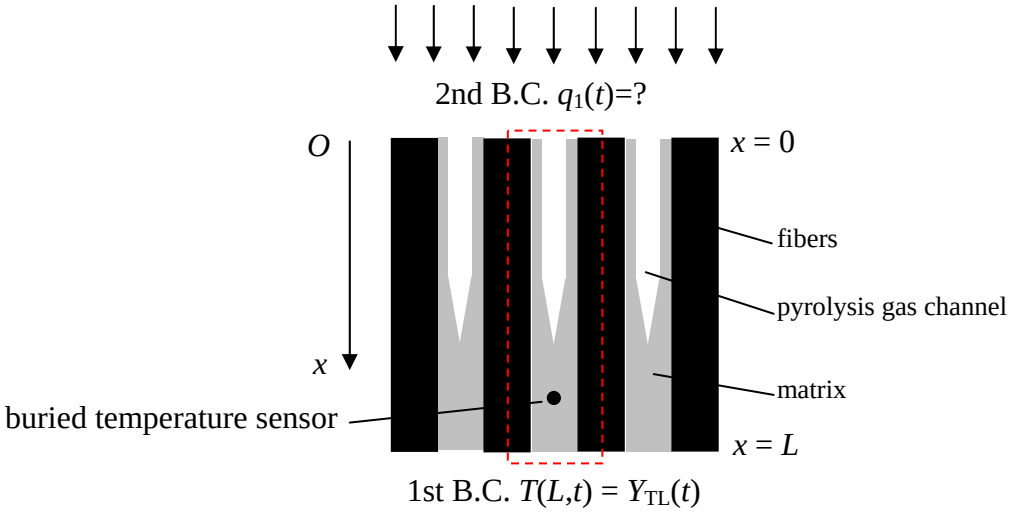

Figure 1 Physical model

The thermal conductivity, *k*, is temperature-dependent and will change as pyrolysis goes on [23]. The volume specific heat, *C*, is calculated by combining the corresponding values of the fibers and matrix, depending on the fraction of the decomposed material [24]:

$$C = (1-\alpha_{\max})C_f + \alpha_{\max} C_m \quad \text{in nonpyrolysis region} \tag{5}$$

$$C = (1-\alpha_{\max})C_f + (\alpha_{\max}-\alpha)C_m \quad \text{in pyrolysis region} \tag{6}$$

where α is the volumetric fraction of the decomposed material with a maximum value of $\alpha_{\max}$ due to the existence of the non-pyrolyzable fibers. The subscripts *f* and *m* denote the fiber and matrix, respectively. Since the volume specific heat *C* is determined by the fraction of the decomposed material, it is also temperature-dependent in nature. All the temperature-dependent thermophysical properties make the IHCP a nonlinear problem.

Pyrolysis is a rate-dependent process. Before the local temperature reaches the pyrolysis point, the fraction α is set to be zero. After the pyrolysis begins, it is obtained by

$$\frac{d\alpha}{dt} = A(1-\alpha)^M e^{B/T} \tag{7}$$

where *A* is the frequency factor; *B* is a parameter related to activation energy; *M* is the order of decomposition chemical reaction. In this work, the chemical reaction is considered to be of first order, which means *M* = 1.

Likewise, before the local temperature reaches the pyrolysis temperature, the heat source term $Q(x,t)$ in Eq. (1) due to pyrolysis decomposition is set to be zero. After the pyrolysis begins, it is determined by

$$Q(t) = -\frac{\rho_f \Delta H}{1-\alpha}\frac{d\alpha}{dt} = -\frac{\rho_f \Delta H}{(1-\alpha)} A e^{\frac{B}{T}-M\int_{t_{pyro}}^{t} Ae^{\frac{B}{T}}dt} \tag{8}$$

where ΔH is the chemical reaction heat.

The other heat source due to the convective heat exchange between the pyrolysis gas and the solid part, $G(x,t)$, is computed as:

$$G(t) = \frac{h_{gas}(T_g - T)}{R_f^2(1-\alpha)/2R_c} \tag{9}$$

where T_g is the temperature of the pyrolysis gas; R_f is the outer radius of the fiber; R_c is the radius of the gas flow channel; h_{gas} is the convection heat coefficient between the gaseous byproducts and the solid part of the composite. The heat transfer coefficient h_{gas} and gas temperature T_g are determined by the gas flow simulation results. In this study, the pyrolysis gas flow is simulated based on a generalized one-dimensional analysis technique for compressible flow with friction and heat transfer described by Shapiro [25], which is briefly summarized as follows.

The temperature of the pyrolysis gas T_g is calculated through the Reynolds Analogy:

$$dT_{g0} = 2 f_r \frac{dx}{D}(T_s - T_{g0}) \tag{10}$$

$$T_g = T_{g0} - \frac{\upsilon_g^2}{2c_{pg}} \tag{11}$$

where T_{g0} is the gas stagnation temperature; f_r is the friction factor; *D* is the diameter of the gas flow channel (*D*=2 R_c); c_{pg} is the mass specific heat of gas at constant pressure; υ_g is the gas velocity, which is estimated based on the Mach number (*Ma*):

$$dMa^2 = \left(F_{T_0} + \frac{2T_{g0}}{T_w - T_{g0}}F_f\right)\frac{dT_{g0}}{T_{g0}} \tag{12}$$

$$\upsilon_g = Ma\sqrt{\kappa R_g T_g} \tag{13}$$

where κ is the specific heat ratio of the pyrolysis gas; R_g is the gas constant; F_f and F_{T_0} are two functions of the Mach number *Ma*; and κ is the specific heat ratio [26].

The convection heat transfer coefficient h_{gas} is computed by the convection correlation formula for channel flow [27]:

$$Nu_D = 0.027\,\mathrm{Re}_D^{4/5}\,\mathrm{Pr}^{1/3}\left(\frac{\mu}{\mu_s}\right)^{0.14} \tag{14}$$

where the Nusselt number $Nu_D = h_{gas}D/k_{gas}$.

In the above-described direct problem, the front-surface heat flux $q_1(t)$ and back-surface temperature $Y_{TL}(t)$ are regarded as known quantities. The purpose of the direct problem is to determine the transient temperature distribution in the composite slab.

2.2 Inverse problem

For the inverse problem, the observed heat flux at the front surface, $q_1(t)$, is treated as unknown and needs to be recovered. The back-surface temperature measurement, $Y_{TL}(t)$, is used as the boundary condition at the back surface.

The inverse problem can be mathematically described as:

$$C(T)\frac{\partial T}{\partial t} = \frac{\partial}{\partial x}\left[k(T)\frac{\partial T}{\partial x}\right] + Q(x,t) + G(x,t) \tag{15}$$

$$T = T_0 \quad \text{for} \quad 0 \le x \le L, \quad t = 0 \tag{16}$$

$$T(L,t) = Y_{TL}(t) \quad \text{for} \quad x = L,\ t > 0 \tag{17}$$

The heat flux readings at the back surface, $Y_{qL}(t)$, and the temperature readings (if necessary) at an interior location x_1, $Y_{T1}(t)$, are considered available as additional information, and will be used in the objective function.

2.3 Sensitivity problem

In order to develop the sensitivity problem, we assume that the unknown heat flux $q_1(t)$ is perturbed by an amount $\xi\Delta q_1(t)$. Thus, the temperature *T*(*x*, *t*) undergoes a variation $\xi\Delta T(t)$, that is:

$$T_\xi(x,t) = T(x,t) + \xi\Delta T(x,t) \tag{18}$$

where ξ is a real number and, as a subscript, ξ is referred to as a perturbed variable. Due to the nonlinear nature of the problem, the perturbation of temperature causes variations on the temperature-dependent properties. The resulting perturbed quantities are linearized as:

$$C_\xi(T_\xi) = C(T) + \frac{dC}{dT}\xi\Delta T \tag{19}$$

$$k_\xi(T_\xi) = k(T) + \frac{dk}{dT}\xi\Delta T \tag{20}$$

For the convenience in the subsequent analysis, we write the differential equation (1) as:

$$D(T) = C(T)\frac{\partial T}{\partial t} - \frac{\partial}{\partial x}\left[k(T)\frac{\partial T}{\partial x}\right] - Q(x,t) - G(x,t) \tag{21}$$

The perturbed form of this equation is:

$$D_\xi(T_\xi) = C_\xi(T_\xi)\frac{\partial T_\xi}{\partial t} - \frac{\partial}{\partial x}\left[k_\xi(T_\xi)\frac{\partial T_\xi}{\partial x}\right] - Q(x,t) - G(x,t) \tag{22}$$

To formulate the sensitivity problem, we apply a limiting process to the differential equations (21) and (22) in the form:

$$\lim_{\xi\to 0}\frac{D_\xi(T_\xi) - D(T)}{\xi} = 0 \tag{23}$$

and similar limiting process are applied for the boundary and initial conditions of the direct problem. After some manipulations, the following sensitivity problem is generated for the determination of the sensitivity function $\Delta T(x,t)$:

$$\frac{\partial(C\Delta T)}{\partial t} = \frac{\partial^2(k\Delta T)}{\partial x^2} \tag{24}$$

$$\Delta T(x,0) = 0 \quad \text{for} \quad 0 \le x \le L, \quad t = 0 \tag{25}$$

$$-\frac{\partial(k\Delta T)}{\partial x} = \Delta q_1(t) \quad \text{for} \quad x = 0,\ t > 0 \tag{26}$$

$$\Delta T(x,t) = 0 \quad \text{for} \quad x = L,\ t > 0 \tag{27}$$

2.4 Adjoint problem

The solution of the inverse problem is to be obtained in such a way that the following objective function is minimized:

$$S[q_1(t)] = \int_0^{t_f}\{Y_{qL}(t) - q[L,t;q_1(t)]\}^2 dt + \int_0^{t_f}\{Y_{T1}(t) - T[x_1,t;q_1(t)]\}^2 dt \tag{28}$$

where t_f is the final simulation time; $Y_{qL}(t)$ and $q[L,t;q_1(t)]$ are the measured and computed heat fluxes at the back surface, respectively; $Y_{T1}(t)$ and $T[x_1,t;q_1(t)]$ are the measured and computed temperatures at the interior location x_1, respectively.

The right hand side of equation (21) is multiplied by a Lagrange multiplier $\lambda(x,t)$ and then integrated over the time and space domains. The resulting expression is added to equation (28) to obtain:

$$S[q_1(t)] = \int_0^{t_f}\{Y_{qL}(t) - q[L,t;q_1(t)]\}^2 dt + \int_0^{t_f}\{Y_{T1}(t) - T[x_1,t;q_1(t)]\}^2 dt + \int_{x=0}^{L}\int_{t=0}^{t_f}\left\{C(T)\frac{\partial T}{\partial t} - \frac{\partial}{\partial x}\left[k(T)\frac{\partial T}{\partial x}\right] - Q(x,t) - G(x,t)\right\}\lambda\, dx dt \tag{29}$$

The above extended functional $S[q_1(t)]$ undergoes a variation $\Delta S[q_1(t)]$ when the unknown quantity $q_1(t)$, the temperature T, the heat flux q, volume specific heat C, thermal conductivity k undergo variations $\xi\Delta q_1(t)$, $\xi\Delta T(t)$, $\xi\Delta q(t)$, $\frac{dC}{dT}\xi\Delta T$, $\frac{dk}{dT}\xi\Delta T$, respectively.

The variation $\Delta S[q_1(t)]$ can be conveniently obtained by applying the following limiting process:

$$\Delta S[q_1(t)] = \lim_{\xi\to 0}\frac{S_\xi[q_1(T)_\xi] - S[q_1(T)]}{\xi} \tag{30}$$

where the term $S_\xi[q_1(T)_\xi]$ is obtained by writing equation (29) for the perturbed quantities defined by equations (18)~(20).

After doing some integration manipulations and applying the boundary and initial conditions of the sensitivity problems and letting the terms containing $\Delta T(x,t)$ be equal to zero, we get the adjoint problem as follows:

$$C\frac{\partial\lambda}{\partial t} + k\frac{\partial^2\lambda}{\partial x^2} + 2\{q[x,t;q_1(t)] - Y_{qL}(t)\}\frac{\Delta q[x,t;q_1(t)]}{\Delta T[x,t;q_1(t)]}\delta(x-L) + 2\{T[x_1,t;q_1(t)] - Y_{T1}(t)\}\delta(x-x_1) = 0$$

in $0 < x < L$, for $t > 0$ (31)

$$\lambda(x,t_f) = 0 \quad \text{in } 0 < x < L, \text{ for } t = t_f \tag{32}$$

$$\frac{\partial\lambda(0,t)}{\partial t} = 0 \quad \text{at } x = 0, \text{ for } t > 0 \tag{33}$$

$$\lambda(L,t) = 0 \quad \text{at } x = L, \text{ for } t > 0 \tag{34}$$

2.4 Gradient equation and iterative procedure

The gradient equation is as follows:

$$\nabla S[q_1(t)] = -\lambda(0,t) \tag{35}$$

The iterative procedure to obtain a convergent inverse solution $q_1(t)$ is:

$$q_1^{k+1}(t) = q_1^k(t) - \beta^k d^k(t) \tag{36}$$

where k is iterative level; β^k is search step size; $d^k(t)$ is the direction of descent, which can be calculated as:

$$d^k(t) = \nabla S[q_1^k(t)] + \gamma^k d^{k-1}(t) \tag{37}$$

where γ^k is conjugate coefficient.

The calculation methods for the conjugate coefficient γ^k and the search step size β^k can be computed as [5]:

$$\gamma^k = \frac{\int_{t=0}^{t_f}\nabla S[g_1^k(t)]\{\nabla S[g_1^k(t)] - \nabla S[g_1^{k-1}(t)]\}dt}{\int_{t=0}^{t_f}\{\nabla S[g_1^{k-1}(t)]\}^2 dt} \quad \text{and} \quad \gamma^0 = 0 \quad \text{for } k = 0 \tag{38}$$

$$\beta^k = \frac{\int_{t=0}^{t_f}\{q[L,t;d^k(t)] - Y_{qL}(t)\}\Delta q[L,t;d^k(t)]dt + \int_{t=0}^{t_f}\{T[x_1,t;d^k(t)] - Y_{T1}(t)\}\Delta T[x_1,t;d^k(t)]dt}{\int_{t=0}^{t_f}\{\Delta q[L,t;d^k(t)]\}^2 dt + \int_{t=0}^{t_f}\{\Delta T[x_1,t;d^k(t)]\}^2 dt} \tag{39}$$

2.5 Stopping criterion

The discrepancy principle is used as the stopping criterion [4, 5]:

$$S[q_1(t)] < \chi \tag{40}$$

where χ denotes the tolerance. Assume that the absolute values of the heat flux residuals and the temperature residuals can be approximated by:

$$\left|Y_{qL}(t) - q[L,t;q_1(t)]\right| \approx \delta_q \quad (41)$$

$$\left|Y_{T1}(t) - T[x_1,t;q_1(t)]\right| \approx \delta_T \quad (42)$$

where δ_q and δ_T is the standard deviations of the heat flux measurement and temperature measurement, respectively. Substituting Eqs. (41) and (42) into Eq. (28), the tolerance χ for the stopping criterion is obtained:

$$\chi = (\delta_q^2 + \delta_T^2)\cdot t_f \quad (43)$$

3. COMPUTATIONAL PROCEDURE

The solution procedure of the above nonlinear IHCP using the CGM is summarized as follows. Start with an initial guess $q_1^0(t)$ for $q_1(t)$, set $k = 0$, and then perform the steps below:

Step 1. Solve the direct problem given by Eqs. (1) ~ (4) for $T(x,t)$ based on the value $q_1^k(t)$.

Step 2. Check the stopping criterion Eq. (40). Stop the iteration if satisfied. Otherwise, continue the following solution procedure.

Step 3. Solve the adjoint problem given by Eqs. (31) ~ (34) for $\lambda(x,t)$.

Step 4. Compute the gradient of the functional $\nabla S[q_1(t)]$ from Eq. (35).

Step 5. Compute the conjugate coefficient γ^k and the direction of descent $d^k(t)$ from Eqs. (38) and (37), respectively.

Step 6. Set $\Delta q_1^k(t) = d^k(t)$ and solve the sensitivity problem given by Eqs. (24)~(27) for $\Delta T(x,t)$ and then $\Delta q(x,t)$.

Step 7. Compute the search step size β^k using Eq.(39).

Step 8. Compute the new estimation for $q_1^{k+1}(t)$ from Eq. (36) and then return to Step 1.

4. RESULTS AND DISCUSSION

4.1 Generation of measurement data

Instead of conducting actual experiment, the measurement data of temperature and heat flux are generated numerically by solving the direct problem described by the governing equation (1) with initial condition given by Eq. (2) and the following boundary conditions:

$$-k\frac{\partial T}{\partial x} = q - h(T - T_\infty) - \varepsilon\sigma(T^4 - T_\infty^4) \quad \text{for} \quad x = 0,\ t > 0 \quad (44)$$

$$-k\frac{\partial T}{\partial x} = h(T - T_\infty) + \varepsilon\sigma(T^4 - T_\infty^4) \quad \text{for} \quad x = L,\ t > 0 \quad (45)$$

where q is the periodic heat flux imposed on the front surface; ε is surface emissivity; σ the Stefan-Boltzmann constant. The results are obtained with the validated computer code [24]. In the inverse heat transfer analysis, the simulated measurement data of back surface temperature and heat fluxes are used as the boundary condition and employed in the objective function, respectively, to estimate the heat flux and temperature at the front surface. These recovered heat flux and temperature will be compared with the front-surface temperature and heat flux calculated from the above direct problem (i.e. Eqs.(1), (2), (44) and (45)) to examine the accuracy of the present inverse heat conduction algorithm.

The simulated measurement data computed from Eqs. (1), (2), (44) and (45) provide the exact (errorless) measurement. To account for the measurement error in back surface heat flux, we add an error term to $Y_{qLexact}(t)$ in the form:

$$Y_{qL}(t) = Y_{qLexact}(t) + \omega\delta_q \quad (46)$$

where $Y_{qLexact}(t)$ is the data simulated from the direct problem described by Eqs. (1), (2), (44) and (45); as mentioned earlier, δ_q is the standard deviation of the heat flux measurement and is set as a percentage of the highest heat flux value at the back surface; ω is a random variable between -1 and 1 generated by the Mersenne Twister method [28].

The bias error in heat flux measurement is ignored. In addition, we assume that the temperature readings at back surface and interior locations contain no errors since temperature can be measured with much less uncertainty compared to the heat flux [8, 9].

4.2 Results of IHCP

The temperature-dependent thermal conductivities of the composite material [23] are listed in Table 1. The thermal conductivities at temperatures between any two data points are obtained by linear interpolation. The density and mass specific heat are 1200 kg/m^3 and 1500 J/(kg·K), respectively for fiber and are 800 kg/m^3 and 1200 J/(kg·K), respectively for the matrix. Other parameters are: L = 2.5 mm, T_0 = 300 K, T_∞ =300 K, h =5 W/(m^2 • K), R_f =400μm, $\alpha_{\max}$ =0.4. The front surface heat flux is assumed to be $q = q_c + 0.1q_c\sin(2\pi ft)$ (W/m^2), where q_c is a constant heat flux, and f is the frequency of the sinusoidal component. Unless specified otherwise, q_c = 200 W/cm^2, and $\delta_q = 5\%\cdot[Y_{qLexact}(t)]_{\max}$.

Table 1 Thermal conductivities of composites as a function of temperature [23]

Temperature, K	Thermal conductivity, W/(m·K)
283	0.01
797	0.5
1087	0.173
3590	0.064

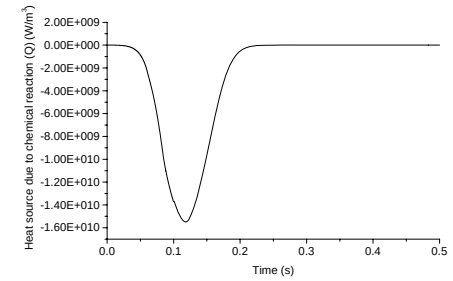

(a)

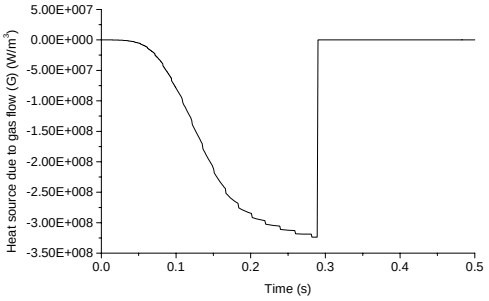

(b)

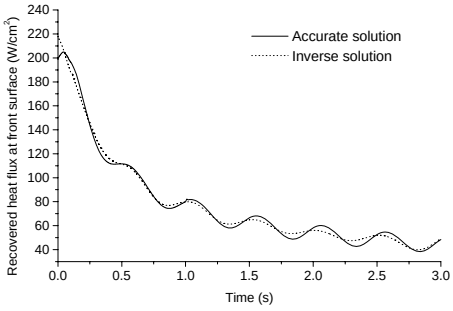

(c)

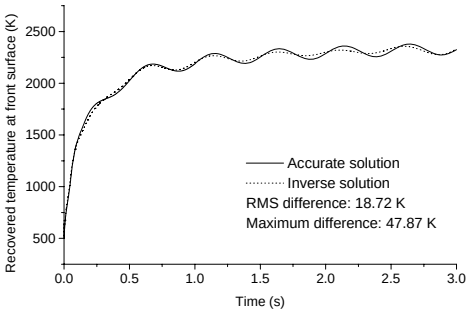

(d)

Figure 2 Inverse solutions for the case where single interior temperature sensor is used ($x_1 = L/3$) and the frequency of the periodic laser heating is f = 2 Hz: (a) Heat source $Q(0, t)$ due to decomposition chemical reaction; (b) Heat source $G(0, t)$ due to pyrolysis gas flow; (c) Recovered front-surface heat flux; (d) Recovered front-surface temperature.

The thermal properties of the pyrolysis gas are considered to be those of CO_2 [29]. The parameters of decomposition chemical reaction are as follows: The pyrolysis onset temperature is $T_{pyro} = 625K$; decomposition reaction heat is $\Delta H = 2\times10^6\ J/kg$; the order of the decomposition reaction is M = 1; the frequency factor in the rate equation is A = 1.243×10^7, constant B in the rate equation is: B = -1.17×10^4 K.

4.2.1 Single interior temperature sensor

Figure 2 shows the inverse heat conduction results for the case where the location of the single interior temperature sensor is $x_1 = 1/3L$ and the frequency of the periodic laser heat flux is f = 2 Hz. Figures 2 (a) and (b) show the heat sources $Q(0, t)$ and $G(0, t)$ due to decomposition chemical reaction and pyrolysis gas flow, respectively. As can be seen, the peak value of heat source $Q(x, t)$ due to chemical reaction takes place at about 0.1 sec while the gas flow heat source peak occurs at some later time (about 0.3 sec). The time delay between these two heat sources can be explained as follows. According to Eq. (8), the heat source $Q(x, t)$ due to chemical reaction is determined by temporal change rate of the fraction of decomposed material $d\alpha/dt$ while the heat source $G(x, t)$ arising from pyrolysis gas flow depends on the absolute value of α based on Eq. (9) (the higher the fraction α, the larger the heat source $G(x, t)$). The maximum rate $d\alpha/dt$ happens at some point in the interval $\alpha = 0 - \alpha_{\max}$, but the highest value of α appears at the end of pyrolysis process ($\alpha = \alpha_{\max}$). As is also seen, both heat sources are negative values, which indicates that the decomposition chemical reaction is endothermic in nature and the gas flow functions as a heat sink that continuously takes heat away from the material.

It is also seen that the recovered front-surface heat flux (Fig. 2(c)) and temperature (Fig. 2(d)) agree well with the direct solutions obtained by solving Eqs. (1), (2), (44) and (45). The maximum difference between the recovered temperature and the accurate solution is 47.87 K, about 2%.

Thermal conductivities of composite materials are usually very low. For the material discussed here, the thermal conductivity ranges from 0.01 W/(m·K) to 0.5 W/(m·K), which is very close to that of a thermally insulated material. Under this circumstance, the inverse problem becomes severely ill-posed, and it is very difficult, if not impossible, to recover the front-surface heating condition just based on the back-surface heat flux or/and temperature measurements. For the simulation case shown in Fig. 2, the temperature measurement at an interior location is indispensable; otherwise, convergent solution cannot be obtained.

Our numerical experiments also show that the frequency of the periodic laser heating flux, f, plays a dominant role in the inverse solution accuracy. The higher the frequency, the more difficult to obtain a convergent inverse solution. As the frequency of the periodic laser heating flux increases, a

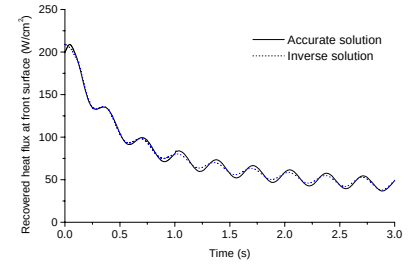

(a)

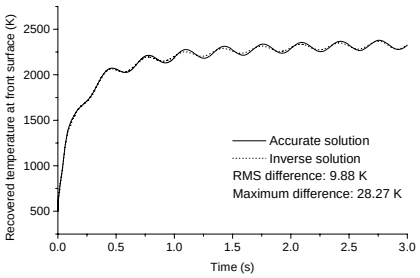

(b)

Figure 3 Inverse solutions for the case where single interior temperature sensor is used ($x_1 = L/5$) and the frequency of the periodic laser heating is f = 3 Hz. (a) Recovered front-surface heat flux; (b) Recovered front-surface temperature.

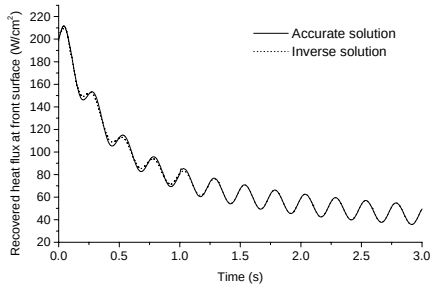

(a)

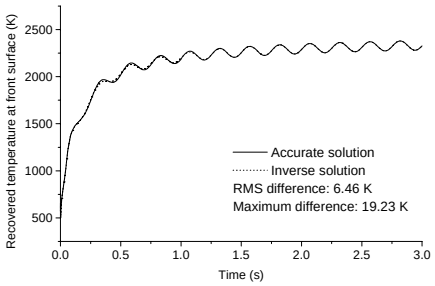

(b)

Figure 4 Inverse solutions for the case where single interior temperature sensor is used ($x_1 = L/8$) and the frequency of the periodic laser heating is f = 4 Hz. (a) Recovered front-surface heat flux; (b) Recovered front-surface temperature.

convergent inverse solution can only be obtained when the interior temperature sensor is moved closer toward the laser heating surface.

Figure 3 gives the recovered heat flux and temperature at front surface when the frequency is increased to f = 3 Hz. The interior temperature sensor is located at $x_1 = L/5$. The convergent solution cannot be obtained if the depth of the temperature sensor is deeper than L/5.

When the frequency of the periodic laser heating flux is further increased to 4Hz, the interior temperature sensor needs to be further moved toward the laser heating surface. Figure 4 shows the recovered heat flux and temperature at front surface when the frequency is 4 Hz. The interior temperature sensor is located at $x_1 = L/8$. Again, the convergent solution cannot be obtained if a temperature sensor is at locations deeper than $L/8$.

Figure 5 presents the recovered heat flux and temperature at front surface for the case where the frequency of the periodic laser heating flux is elevated to 5 Hz. The interior temperature sensor is located at $x_1 = L/10$. The convergent solution cannot be obtained when a temperature sensor located at a depth deeper than $L/10$.

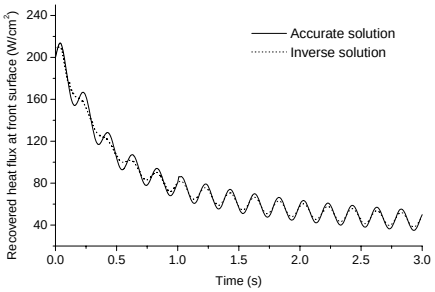

(a)

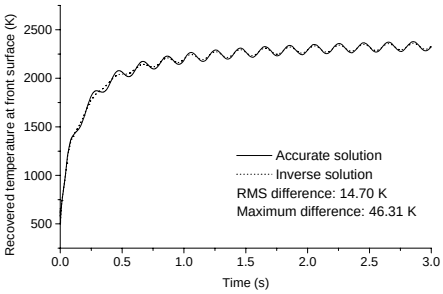

(b)

Figure 5 Inverse solutions for the case where single interior temperature sensor is used ($x_1 = L/10$) and the frequency of the periodic laser heating is f = 5 Hz. (a) Recovered front-surface heat flux; (b) Recovered front-surface temperature.

4.2.2 Two interior temperature sensors

All of the foregoing simulations are performed for the case where only one single interior temperature sensor is installed.

For inverse heat conduction problems, it is generally recognized that multiple sensor measurement information can give more accurate inverse solutions. The extension of the computational model from single-interior-temperature-sensor case to two-interior-temperature-sensors case is quite straightforward. For brevity, the detailed derivations of equations are not given here.

Figure 6 shows the inverse solutions for the case where two interior temperature sensors are used. One is located at $x_1 = L/3$, and the other is located at $x_2 = 2L/3$. The frequency of the periodic laser heating flux is 5Hz. It can be seen in Fig. 6 that the oscillating character in the periodic laser heating cannot be correctly recovered even if two interior temperature sensors are used, because they are buried too deeply. This implies that moving the embedded temperature sensor toward the front surface is the most efficient way to recover the high-frequency periodic heat flux at front surface for low thermal-conductivity composites.

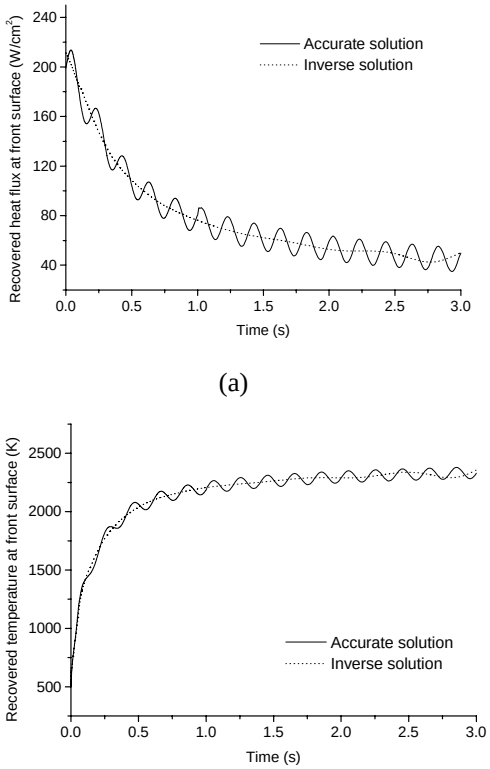

(a)

(b)

Figure 6 Inverse solutions for the case where double interior temperature sensors are used ($x_1 = L/3, x_2 = 2L/3$) and the frequency of the periodic laser heating is f = 5 Hz. (a) Recovered front-surface heat flux; (b) Recovered front-surface temperature.

4.2.3 Simulation on the case where the thermal properties include random errors

In practice, random errors exist not only in the measurement of heat flux but also in the measurement of thermophysical properties. This means that the thermophysical properties are not just temperature-dependent but also contain random errors. This further adds to the nonlinear and ill-posed complexities of the inverse problem. Figure 7 shows the results for the composite material whose thermal properties (thermal conductivity and specific heat) contains 5% random errors. The frequency of the periodic laser heating flux is 5 Hz. A single interior temperature sensor located at $x_1 = L/10$ is used. It is seen that the inverse algorithm and the numerical model formulated in this study have very good performance in handling this type of problems where error-containing thermal properties are involved.

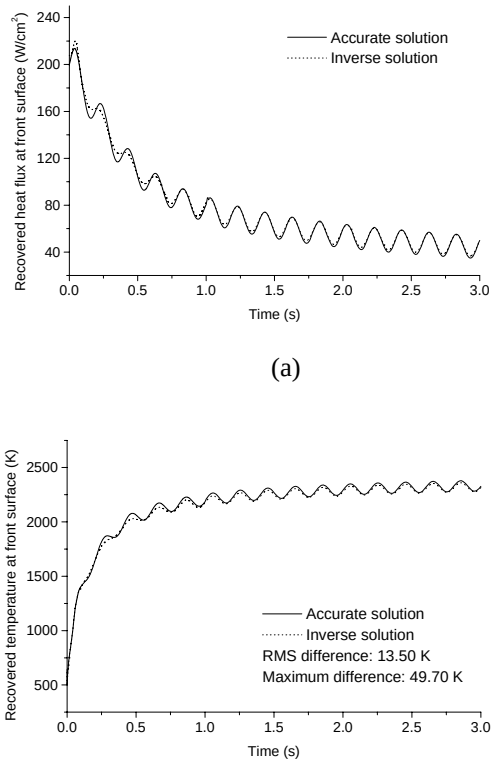

(a)

(b)

Figure 7 Inverse solutions for composite material whose thermal properties include 5% random errors (frequency f = 5 Hz, single interior temperature sensor is used at $x_1 = L/10$). (a) Recovered front-surface heat flux; (b) Recovered front-surface temperature.

5. CONCLUSIONS

In this work, a new inverse numerical model is developed to recover the periodic heating condition at the front surface of a low-thermal-conductivity composite material using the back-surface temperature and heat flux measurements as well as interior temperature readings. The pyrolysis chemical reaction and outgassing flow effects are well incorporated. It is found that for the low-thermal-conductivity composite materials, the inverse heat conduction problem becomes severely ill-posed, and it is necessary to measure the temperatures at interior locations as additional information to recover the front-surface periodic heating condition. Our numerical experiments showed that the frequency of the periodic laser heating flux plays a dominant role in the inverse solution accuracy. When the frequency of the periodic laser heating flux is high, a convergent inverse solution can only be achieved when the interior temperature sensor is located at a shallow depth. The optimum sensor locations are suggested for a variety of cases that have different heating frequencies. Simulations are also performed to test the case where dual interior temperature sensors are installed. The results showed that even with two interior temperature sensors the oscillating characteristic in the periodic laser heating cannot be correctly reconstructed if the locations of these two sensors are far away from the laser heating surface. This implies that moving the embedded temperature sensor toward the laser heating surface is the most efficient way to recover the high-frequency periodic heat flux at the front surface of a low-thermal-conductivity composite material. The robustness of the proposed inverse algorithm and numerical strategies are also demonstrated by its strong ability in handling the case of thermal properties with random errors.

ACKNOWLEDGMENTS

The authors would like to thank the Test Resource Management Center (TRMC) Test and Evaluation/Science & Technology (T&E/S&T) Program for their support. This work is funded by the T&E/S&T Program through the U.S. Army Program Executive Office for Simulation, Training and Instrumentation's contract number W900KK-08-C-0002. The authors would also like to express their gratitude to Dr. James L. Griggs for his valuable discussions.

REFERENCES

[1] Agarwal, B. D., and Broutman, L. J., *Analysis and Performance of Fiber Composites*, 2nd ed., John Wiley and Sons, New York, 1990.

[2] dell'Erba, M., Galantucci, L. M., and Miglietta, S., "An Experimental Study on Laser Drilling and Cutting of Composite Materials for the Aerospace Industry Using Excimer and CO_2 Sources," *Composites Manufacturing*, Vol.3, No.1, 1992, pp.14-19.

[3] Beck, J. V., Blackwell, B., and St-Clair, C. R., *Inverse Heat Conduction: Ill Posed Problems*, Wiley, New York, 1985.

[4] Alifanov, O. M., *Inverse Heat Transfer Problems*, Springer-Verlag, Berlin/Heidelberg, 1994.

[5] Özisik, M. N., and Orlande, H. R. B., *Inverse Heat Transfer: Fundamentals and Applications*, Taylor & Francis, New York, 2000.

[6] Diller, T. E., "Advances in heat flux measurements," *Advances in Heat Transfer*, Vol. 23, 1993, pp. 279-368.

[7] Childs, P. R. N., Greenwood, J. R., and Long, C. A., "Heat flux measurement techniques," *Proceedings of the Institute of Mechanical Engineers. Part C: Journal of Mechanical Engineering Science*, Vol. 213, No. C7, 1999, pp. 655-677.

[8] Tong, A., "Improving the accuracy of temperature measurements," *Sensor Review*, Vol. 21, No. 3, 2001, pp. 193-198.

[9] Childs, P. R. N., "Advances in temperature measurement," *Advances in Heat Transfer*, Vol. 36, 2002, pp. 111-181.

[10] Saidi, A., and Kim, J., "Heat flux sensor with minimal impact on boundary conditions," *Experimental Thermal and Fluid Science*, Vol. 28, 2004, pp. 903-908.

[11] Loulou, T., and Scott, E. P., "An inverse heat conduction problem with heat flux measurements," *International Journal for Numerical Methods in Engineering*, Vol. 67, 2006, pp. 1587-1616.

[12] Sparrow, E. M., Haji-Sheikh, A., and Lundgren, T. S., "The inverse problem in transient heat conduction," *ASME Journal of Applied Mechanics*, Vol.86, 1964, pp. 369-375.

[13] Jarny, Y., Özisik, M. N., and Bardon, J. P., "A general optimization method using adjoint equation for solving multidimensional inverse heat conduction," *International Journal Heat and Mass Transfer*, Vol.34, 1991, pp. 2911-2919.

[14] Pasquetti, R., Niliot, C. L., "Boundary element approach for inverse heat conduction problems: application to a bidimensional transient numerical experiment," *Numerical Heat Transfer, Part B*, Vol. 20, 1991, pp. 169-189.

[15] Yang, C. -Y. , and Chen, C. –K., "The boundary estimation in two-dimensional inverse heat conduction problems," *Journal of Physics D: Applied Physics*, Vol. 29, 1996, pp. 333-339.

[16] Huang, C. –H, and Wang, S. –P., "A three-dimensional inverse heat conduction problem in estimating surface heat flux by conjugate gradient method," *International Journal of Heat and Mass Transfer*, Vol. 42, 1999, pp. 3387-3403.

[17] Emery, A. F., Nenarokomov, A. V., and Fadale, T. D., "Uncertainties in parameter estimation: the optimal experimental design," *International Journal of Heat and Mass Transfer*, Vol. 43, 2000, pp. 3331-3339.

[18] Monde, M., Arima, H., and Mitsutake, Y., "Estimation of surface temperature and heat flux using inverse solution

for one-dimensional heat conduction," *ASME Journal of Heat Transfer*, Vol. 125, 2003, pp. 213-223.

[19] Xue, X., Luck, R., and Berry, J. T., "Comparisons and improvements concerning the accuracy and robustness of inverse heat conduction algorithms," *Inverse Problems in Science and Engineering*, Vol. 13, No. 2, 2005, pp. 177-199.

[20] Frankel, J. I., Osborne, G. E., and Taira, K., "Stabilization of ill-posed problems through thermal rate sensors," *AIAA Journal of Thermophysics and Heat Transfer*, Vol. 20, No. 2, 2006, pp. 238-246.

[21] Zhou, J., Zhang, Y., Chen, J. K., and Feng, Z. C., "Inverse heat conduction in a finite slab with measured back heat flux," *Proceedings of the 47th AIAA Aerospace Sciences Meeting*, Orlando, FL., January 5-9, 2009.

[22] Zhou, J., Zhang, Y., Chen, J. K., and Feng, Z. C., "Inverse estimation of surface heating condition in a finite slab with temperature-dependent thermophysical properties," *Inverse Problems in Science and Engineering*, Submitted.

[23] Chen, J. K., Perea, A., and Allahdadi, F. A., "A study of laser/composite material interactions," *Composites Science and Technology*, Vol. 54, 1995, pp. 35-44.

[24] Zhou, J., Zhang, Y., Chen, J. K., and Smith, D. E., "A non-equilibrium thermal model for rapid heating and pyrolysis of organic composites," *ASME Journal of Heat Transfer*, Vol. 130, 2008, pp. 064501.

[25] Shapiro, A. H., *The Dynamics and Thermodynamics of Compressible Fluid Flow*, Vol. 1, Ronald Press Company, New York, 1953.

[26] Smith, D. E., Zhang, Y., and Chen, J. K., *HELVAMP: Laser/Composite Interaction Research Project*, Final Technical Report Submitted to Air Force Research Laboratory/Ball Aerospace, July, 2006.

[27] Kays, W. M., and Crawford, M. E., *Convective Heat and Mass Transfer*, McGraw-Hill, New York, 1980.

[28] Matsumoto, M., and Nishimura, T., "Mersenne Twister: a 623-dimensionally equidistributed uniform pseudorandom number generator," *ACM Transactions on Modeling and Computer Simulation*, Vol.8, No.1, 1998, pp. 3-30.

[29] Incropera, F. P., Dewitt, D. P., Bergman, T. L., and Lavine, A. S., *Fundamentals of Heat and Mass Transfer*, 6th Ed., John Wiley & Sons, New York, 2007.